An hp adaptive strategy to compute the vibration modes of a fluid-solid coupled system

M.G. Armentano [1] C. Padra [2], R. Rodríguez [3], and M. Scheble[2]

Abstract: In this paper we propose an hp finite element method to solve a two-dimensional fluid-structure vibration problem. This problem arises from the computation of the vibration modes of a bundle of parallel tubes immersed in an incompressible fluid. We use a residual-type a posteriori error indicator to guide an hp adaptive algorithm. Since the tubes are allowed to be different, the weak formulation is a non-standard generalized eigenvalue problem. This feature is inherited by the algebraic system obtained by the discretization process. We introduce an algebraic technique to solve this particular spectral problem. We report several numerical tests which allow us to assess the performance of the scheme.

Keywords: fluid structure interaction, vibration problem, hp finite element adaptive method

1 Introduction

In this work we consider an hp finite element adaptive scheme for solving a fluid-structure interaction problem, which corresponds to computing the vibrations of a bundle of parallel tubes immersed in an incompressible fluid contained in a rigid cavity.

The numerical solution of spectral problems arising in fluid mechanics is a subject of permanent interest; see, for instance, [Morand and Ohayon (1995); Conca, Planchard, and Vanninathan (1995); Bermúdez, Durán, and Rodríguez (1997); Conca, Osses, and Planchard (1998); Bermúdez, Rodríguez, and Santamarina (2000); Armentano, Padra, Rodríguez, and Scheble (2011)] and the references therein. In particular, the topic considered in this paper has its roots in nuclear engineering

[1] Departamento de Matemática, Facultad de Ciencias Exactas y Naturales, Universidad de Buenos Aires, IMAS - Conicet, 1428, Buenos Aires, Argentina.

[2] Centro Atómico Bariloche, 4800, Bariloche, Argentina.

[3] CI^{2}MA, Departamento de Ingeniería Matemática, Universidad de Concepción, Casilla 160-C, Concepción, Chile.

problems such as fluid interaction in vapor generator and nuclear reactor cores and has been studied by several authors [Planchard (1983); Planchard and Ibnou-Zahir (1983); Conca, Osses, and Planchard (1998)]. These problems are related to protecting people and the environment. For instance, according to IAEA Safety Standards [IAEA (2005)], for the operational state, the fuel assembly in nuclear plants should be designed so that they cannot be unacceptably affected by damage due to vibration or fretting.

It is well known that adaptive procedures based on a posteriori error indicators play nowadays a relevant role in the numerical solution of partial differential equations and, in particular, in eigenvalue problems. There are several papers for the classical h version of finite element methods concerning the development of efficient adaptive schemes for different eigenvalue problems, for example, [Durán, Gastaldi, and Padra (1999); Larson (2000); Durán, Padra, and Rodríguez (2003); Armentano and Padra (2008); Lovadina, Lyly, and Stenberg (2009)], and a few recent references regarding the hp finite element solution of this kind of problems [Boffi, Costabel, Dauge, and Demkowicz (2006); Boffi (2007); Azaiez, Deville, Gruber, and Mund (2008)]. However, the bibliography about hp-adaptive schemes for spectral problems is scarce. One of the main difficulties in hp-adaptivity arises from the fact that the accuracy can be improved in two different ways, either by subdividing elements or by increasing the polynomial degree. Thus, at each refinement step, it is necessary to decide which of these two options must be chosen.

In a recent paper [Armentano, Padra, Rodríguez, and Scheble (2011)], we have introduced and analyzed an hp finite element solver for the spectral problem described above. We have proposed an adaptive scheme and applied it to different cavities and shapes of tubes. However, in our error analysis and in all the examples considered in that article, the tubes have been assumed to be geometrically and physically identical, namely, with the same shape, mass and stiffness. The reason for this is that when the tubes are not all identical, the resulting spectral problem is not any longer a standard generalized eigenvalue problem and it is not clear how it could be efficiently solved.

In this paper we propose a strategy to solve this particular algebraic spectral problem. It consists in transforming it into an equivalent standard generalized eigenvalue problem which can be solved with classical eigensolvers. Moreover, such a strategy allows us to extend the results from [Armentano, Padra, Rodríguez, and Scheble (2011)] to derive an hp finite element adaptive method which can be applied to bundles of tubes with different shapes, rigidities and masses. Therefore, we are able to perform a more complete numerical experimentation, which allows us to assess the performance of the proposed adaptive scheme.

The rest of the paper is organized as follows. In Section 2 we recall the fluid-solid

vibration problem and introduce the *hp* finite element method, the a posteriori error estimator and the adaptive refinement strategy. In Section 3 we propose an algorithm to solve the algebraic spectral problem. The algorithm can be efficiently combined with the refinement scheme in such a way that it allows driving the adaptive process by considering the actual singularities of the vibration modes. In Section 4 we report some numerical examples which allow assessing the performance of the adaptive scheme. Finally, we end the paper drawing some conclusions in Section 5.

2 The spectral problem and the *hp* finite element adaptive scheme

We consider a coupled system composed of K elastically mounted parallel tubes immersed in an incompressible fluid inside a rigid cavity. The tubes are assumed to be rigid and only small oscillations of the fluid around the state of rest are allowed. The problem is to determine the free vibration modes of the system.

Under reasonable assumptions [Conca, Planchard, and Vanninathan (1995)], this problem can be posed in a two-dimensional (2D) framework, a planar transverse section of the cavity being its domain. Tube number i is modeled as a harmonic oscillator with stiffness k_i and mass m_i (both per unit length), whereas the fluid is taken as perfectly incompressible with constant density ρ. Assuming an irrotational flow, the velocity field V can be derived from a potential U: $V(x,t) = \nabla_x U(x,t)$.

We call Ω the bounded 2D domain occupied by the fluid, Γ_0 its outer boundary and Γ_i the interfaces between tube number i and the fluid. (See Fig. 1.)

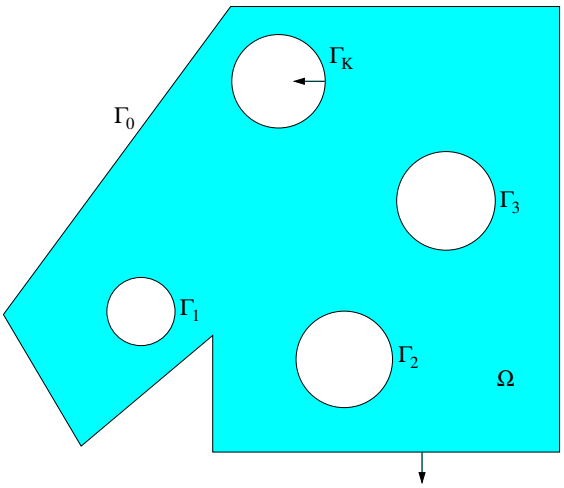

Figure 1: Sketch of the 2D domain

As is usual in vibration models, we seek harmonic solutions of the form $U(x,t) = u(x)e^{i\omega t}$. Then, the problem of computing the vibration modes of the coupled system consists in finding the free vibration frequencies ω and the corresponding amplitudes u of the velocity potential, which has to satisfy the following equations (see Section II.1 from [Conca, Planchard, and Vanninathan (1995)] for its derivation):

$$\Delta u = 0 \qquad \text{in } \Omega, \tag{1}$$

$$\frac{\partial u}{\partial n} = 0 \qquad \text{on } \Gamma_0, \tag{2}$$

$$\left(k_i - m_i\omega^2\right)\frac{\partial u}{\partial n} = \rho\omega^2\left(\int_{\Gamma_i} un\right)\cdot n \quad \text{on } \Gamma_i, \quad i = 1,\ldots,K, \tag{3}$$

where n denotes the unit outer normal to the boundary of Ω.

Let $\mathscr{V} := \left\{v : \Omega \to \mathbb{R} : \int_\Omega \left(|v|^2 + |\nabla v|^2\right) < \infty\right\}$ (i.e., the Sobolev space $H^1(\Omega)$). Multiplying Eq. 1 by a test function $v \in \mathscr{V}$, integrating by parts and using the boundary conditions given by Eq. 2 and Eq. 3, we obtain the following variational formulation of this problem, which holds true as long as $\omega^2 \neq \frac{k_i}{m_i}$ for all $i = 1,\ldots,K$: Find $\omega > 0$ and a non-vanishing $u \in \mathscr{V}$ such that

$$\int_\Omega \nabla u \cdot \nabla v = \sum_{i=1}^{K} \frac{\rho\omega^2}{k_i - m_i\omega^2}\left(\int_{\Gamma_i} un\right)\cdot\left(\int_{\Gamma_i} vn\right) \qquad \forall v \in \mathscr{V}. \tag{4}$$

We note that Eq. 4 is not a standard generalized eigenvalue problem, because there is not a unique eigenvalue multiplying a bilinear form on the right-hand side, but different rational functions of ω multiplying different bilinear forms for each tube.

The existence of solution to this problem has been analyzed in Section II.2.1 from [Conca, Planchard, and Vanninathan (1995)]. It was proved in this reference that Eq. 1 – Eq. 3 attains $2K$ vibration frequencies with corresponding linearly independent eigenfunctions (recall that K is the number of tubes). Let us remark that this finite number of modes is easy to predict, since each rigid tube is perfectly rigid and has only two degrees of freedom, whereas the fluid, being incompressible, cannot have vibration modes. We further assume that the $2K$ free vibration frequencies satisfy $\omega^2 \neq \frac{k_i}{m_i}$ for all $i = 1,\ldots,K$, so that the solutions to Eq. 1 – Eq. 3 are also solutions to Eq. 4, which is the one we are going to discretize.

2.1 The hp finite element method

We introduce an hp finite element method to compute a solution of Eq. 4. Let $\mathscr{T}_h$ be a triangular mesh in Ω such that any two triangles share at most a vertex or an edge. Let h stand for the mesh-size; namely, $h := \max_{T\in\mathscr{T}_h} h_T$, with h_T being the length of the largest edge of the triangle T. We assume that $\mathscr{T}_h$ satisfies a minimum

angle condition or, equivalently, that there exists a constant $\sigma > 0$ such that $\frac{h_T}{\rho_T} \leq \sigma$, where ρ_T is the diameter of the largest circle contained in T. Further, we assume for all meshes, that there is no triangle with vertices lying on two different Γ_i (this will be useful for the procedure that we will propose in Section 3 to solve the generalized eigenvalue problem).

We associate with each element $T \in \mathscr{T}_h$ a (maximal) polynomial degree $p_T \in \mathbb{N}$. We assume that the polynomial degrees of neighboring elements are comparable, i.e., there exists a constant $\gamma > 0$ such that

$$\gamma^{-1} p_T \leq p_{T'} \leq \gamma p_T \qquad \forall T, T' \in \mathscr{T}_h \text{ with } T \cap T' \neq \emptyset. \tag{5}$$

We call $p := \{p_T\}_{T \in \mathscr{T}_h}$ the family of polynomial degrees for each triangle.

Throughout the paper, we will denote by C a generic positive constant, not necessarily the same at each occurrence, which may depend on the mesh and the degree of the polynomials only through the minimal angle and the parameter γ, respectively.

We define the finite element space as follows:

$$\mathscr{V}_h^p := \{v : \Omega \to \mathbb{R} \text{ continuous} : \ v|_T \in \mathscr{P}_{p_T} \ \forall T \in \mathscr{T}_h\} \subset \mathscr{V},$$

where $\mathscr{P}_{p_T}$ denotes the set of polynomials of degree at most p_T. Notice that the definition of $\mathscr{V}_h^p$ allows for different polynomial degrees on each edge of any triangle. Therefore, the space $\left\{ v|_T : \ v \in \mathscr{V}_h^p \right\}$ does not necessarily contain all the polynomials of degree p_T. However, there exists $p'_T \leq p_T$ such that

$$\mathscr{P}_{p'_T} \subset \left\{ v|_T : \ v \in \mathscr{V}_h^p \right\} \subset \mathscr{P}_{p_T} \tag{6}$$

and $p_T / p'_T \leq \gamma$ because of the assumption settled by Eq. 5.

The discrete eigenvalue problem associated with Eq. 4 is the following:

Find ω_h and a non-vanishing $u_h \in \mathscr{V}_h^p$ such that

$$\int_\Omega \nabla u_h \cdot \nabla v_h = \sum_{i=1}^{K} \frac{\rho \omega_h^2}{k_i - m_i \omega_h^2} \left(\int_{\Gamma_i} u_h n \right) \cdot \left(\int_{\Gamma_i} v_h n \right) \qquad \forall v_h \in \mathscr{V}_h^p. \tag{7}$$

Note that we are implicitly assuming that $\omega_h^2 \neq \frac{k_i}{m_i}$ for all $i = 1, \ldots, K$.

For the same reasons as above, this is a non-standard algebraic eigenvalue problem, too. We will show in Section 3 that this particular spectral problem can be reduced to an equivalent well-posed generalized matrix eigenvalue problem, which can be solved with standard techniques.

We have obtained in [Armentano, Padra, Rodríguez, and Scheble (2011)] the following a priori error estimates for the computed vibration frequencies ω_h and the

associated eigenfunctions u_h (which correspond to the velocity potential), in the case that all the tubes have the same mass and stiffness.

Theorem 2.1 *There hold*

$$|\omega - \omega_h| \leq C \left(\max_{T \in \mathscr{T}_h} \frac{h_T}{p_T} \right)^{2r} \qquad \text{and} \qquad \int_\Omega |\nabla u - \nabla u_h|^2 \leq C \left(\max_{T \in \mathscr{T}_h} \frac{h_T}{p_T} \right)^{2r}$$

for all $r < \frac{\pi}{\theta}$, with θ being the largest reentrant angle of Ω.

2.2 A posteriori error estimates

In what follows we introduce an a posteriori indicator for the error of the proposed hp finite element method.

For each inner edge ℓ, we choose a unit normal vector n_ℓ and denote the two triangles sharing this edge T_{in} and T_{out}, with n_ℓ pointing outwards T_{in}. We set

$$\left[\!\left[\frac{\partial u_h}{\partial n} \right]\!\right]_\ell := \nabla \left(u_h|_{T_{\text{out}}} \right) \cdot n_\ell - \nabla \left(u_h|_{T_{\text{in}}} \right) \cdot n_\ell,$$

which corresponds to the jump of the normal derivative of u_h across the edge ℓ. Notice that this value is independent of the chosen direction of the normal vector n_ℓ.

Let us define, for each edge ℓ,

$$J_\ell := \begin{cases} \dfrac{1}{2} \left[\!\left[\dfrac{\partial u_h}{\partial n} \right]\!\right]_\ell, & \text{if } \ell \text{ is an inner edge,} \\ \dfrac{\partial u_h}{\partial n}, & \text{if } \ell \subset \Gamma_0, \\ \dfrac{\partial u_h}{\partial n} - \dfrac{\rho \omega_h^2}{k_i - m_i \omega_h^2} \left(\displaystyle\int_{\Gamma_i} u_h n \right) \cdot n, & \text{if } \ell \subset \Gamma_i, \quad i = 1, \ldots, K. \end{cases}$$

For each element $T \in \mathscr{T}_h$, we define the local error indicator η_T by

$$\eta_T^2 := \frac{h_T^2}{p_T^2} \|\Delta u_h\|_{L^2(T)}^2 + \sum_{\ell \text{ edge of } T} \frac{|\ell|}{p_\ell} \|J_\ell\|_{L^2(\ell)}^2, \tag{8}$$

with $p_\ell := \max \{ p_T : T \supset \ell \}$, and the global error estimator η_Ω by

$$\eta_\Omega^2 := \sum_{T \in \mathscr{T}_h} \eta_T^2.$$

The arguments used in [Armentano, Padra, Rodríguez, and Scheble (2011)] for a similar problem, but with all the tubes having the same mass and stiffness, can be adapted to our case leading to the following a posteriori error estimates.

Theorem 2.2 *i) There exists a positive constant C such that*

$$\int_\Omega |\nabla(u-u_h)|^2 \leq C\left(\eta_\Omega^2+\Lambda_1\right),$$

where

$$\Lambda_1 := \sum_{i=1}^{K}\left|\frac{\rho\omega^2}{k_i-m_i\omega^2}\int_{\Gamma_i} un-\frac{\rho\omega_h^2}{k_i-m_i\omega_h^2}\int_{\Gamma_i} u_h n\right|\left|\int_{\Gamma_i}(un-u_h n)\right|.$$

ii) For all $\delta>0$, there exists a positive constant C_δ such that for all $T\in\mathscr{T}_h$, if T has only inner edges or edges on Γ_0, then

$$\eta_T^2 \leq C_\delta p_T^{2+\delta}\int_{O_T}|\nabla(u-u_h)|^2$$

whereas, if T has an edge lying on Γ_i, $i=1,\ldots,K$, then

$$\eta_T^2 \leq C_\delta p_T^{2+\delta}\left(\int_{O_T}|\nabla(u-u_h)|^2+\Lambda_2\right),$$

where $O_T := \bigcup\{T'\in\mathscr{T}_h:\ T' \text{ and } T \text{ share an edge}\}$ and

$$\Lambda_2 := \frac{h_T^2}{p_T^2}\left|\frac{\rho\omega^2}{k_i-m_i\omega^2}\left(\int_{\Gamma_i} un\right)-\frac{\rho\omega_h^2}{k_i-m_i\omega_h^2}\left(\int_{\Gamma_i} u_h n\right)\right|^2.$$

This theorem yields the reliability of the error estimator η_Ω (up to the term Λ_1) and the efficiency of the error indicator η_T (up to the term Λ_2, for edges lying on the tubes). These two terms, Λ_1 and Λ_2, are very likely higher order. In fact, this is proved in [Armentano, Padra, Rodríguez, and Scheble (2011)] in the case of identical tubes. The proof relies on an a priori error estimate for $\left|\int_{\Gamma_i}(un-u_h n)\right|$, which for identical tubes has been proved in Proposition 3.1 from that reference. To the best of the authors' knowledge, it is still an open question to prove it for tubes with different physical parameters.

2.3 Adaptive refinement strategy

There are several strategies to determine which elements should be refined in an *h*-finite element adaptive scheme. A usual one is the so-called *mean value strategy* in which all the triangles T with $\eta_T \geq \theta\eta_{\mathrm{M}}$ are marked to be refined, where

$$\eta_{\mathrm{M}}^2 := \frac{1}{\#\mathscr{T}_h}\sum_{T\in\mathscr{T}_h}\eta_T^2$$

($\#\mathscr{T}_h$ denotes the number of elements of $\mathscr{T}_h$) and $\theta > 0$ is a parameter which can be arbitrarily chosen.

Our hp adaptive algorithm uses this strategy to mark the triangles to be refined, with the additional consideration that, at each step, for each marked triangle, it has to be decided whether to perform a p-refinement or an h-refinement. In the case of p-refinement, the degree p_T of the marked element is increased by one and the triangle is kept fixed. On the other hand, in the case of h-refinement, the marked element T is subdivided into four triangles, $T = \bigcup_{j=1}^{4} T'_j$, and the degree is kept fixed in the new elements, i.e., $p_{T'_j} = p_T$. Moreover, the conformity of the mesh is preserved by means of a longest edge subdivision strategy on the unrefined neighboring triangles [Verfürth (1996)]. Because of this, it happens that some elements not marked for h-refinement, are subdivided anyway into two or three triangles. Thus, in general, we will have that $T = \bigcup_{j=1}^{k} T'_j$ with $k = 2$, 3 or 4.

In order to decide whether to apply a p or an h refinement to a particular marked triangle, we follow the approach proposed in [Melenk and Wohlmuth (2001)], which is based on the comparison of the current local estimated error with a prediction of this error obtained from the preceding step. If at the preceding step there was an h refinement leading to $T = \bigcup_{j=1}^{k} T'_j$, $k = 2,3,4$, then the prediction indicator is defined as follows:

$$\left(\eta_{T'_j}^{\text{pred}}\right)^2 := \gamma_h \left(\frac{|T_j|}{|T|}\right)^{p_T+1} \eta_T^2,$$

where γ_h is a control parameter that must be determined in advance. On the other hand, if at the preceding step there was a p refinement on the element T, then the prediction indicator is defined by

$$\left(\eta_T^{\text{pred}}\right)^2 := \gamma_p \eta_T^2,$$

where $\gamma_p \in (0,1)$ is a reduction factor also chosen in advance. Finally, for those elements neither p nor h refined at the preceding step,

$$\left(\eta_T^{\text{pred}}\right)^2 := \gamma_n \left(\eta_T^{\text{pred}}\right)^2,$$

where γ_n is another parameter chosen in advance, too. In all cases, once η_T^{pred} is computed, we proceed to an h refinement of the marked triangle T when the error indicator η_T is larger than the prediction indicator η_T^{pred} and to a p refinement otherwise.

Altogether, we arrive at the algorithm shown in Tab. 1.

Table 1: Refinement algorithm

If $\eta_T^2 \geq \theta \eta_{\mathrm{M}}^2$ then
  if $\eta_T^2 \geq \left(\eta_T^{\mathrm{pred}}\right)^2$ then
    subdivide T into 4 triangles T_j', $1 \leq j \leq 4$
    longest edge strategy to maintain mesh conformity
    $p_{T_j} := p_T$
    $\left(\eta_{T_j'}^{\mathrm{pred}}\right)^2 := \gamma_h \left(\frac{|T_j|}{|T|}\right)^{p_T+1} \eta_T^2$
  else
    $p_T := p_T + 1$
    $\left(\eta_T^{\mathrm{pred}}\right)^2 := \gamma_p \eta_T^2$
  end
else
  $\left(\eta_T^{\mathrm{pred}}\right)^2 := \gamma_n \left(\eta_T^{\mathrm{pred}}\right)^2$
end

We set $\eta_T^{\mathrm{pred}} := 0$ for all elements T on the initial triangulation, so that the first step is a purely h-refinement on all marked elements.

3 Solution of the non standard matrix eigenvalue problem

In this section we analyze some numerical aspects concerning the solution of the non-standard eigenvalue problem given by Eq. 7.

First notice that the solutions of both, the continuous problem (Eq. 4) and the discrete one (Eq. 7), are determined up to an additive constant. In fact, it is simple to check that if u is a solution of Eq. 4, then $u+c$ is also a solution of the same problem for any constant c and the same vibration frequency ω. This is quite reasonable, since the physical quantity is not u but ∇u. Exactly the same happens with Eq. 7.

To fix uniquely a solution of Eq. 7, it is enough to set its value to zero at a given node of the mesh. With this aim, we choose an arbitrary fixed node $P_0 \in \Gamma_0$ (the same for all meshes in the adaptive process) and restrict the finite element space to the functions in $\mathscr{V}_h^p$ which vanish at that node P_0.

We denote by $\mathscr{N}$ the set of nodes of the finite element space excluding P_0 and decompose it as follows: $\mathscr{N} = \mathscr{N}_1 \cup \mathscr{N}_2$, with $\mathscr{N}_1 = \bigcup_{i=1}^{K} \mathscr{N}^{(i)}$, where $\mathscr{N}^{(i)}$ is the subset of nodes lying on Γ_i, $1 \leq i \leq K$, and $\mathscr{N}_2$ is the subset of the remaining ones

(i.e., the nodes lying either in Ω or on Γ_0).

We denote by M_i the number of nodes of $\mathscr{N}^{(i)}$ ($i = 1,\dots,K$) and by N_j the number of nodes on $\mathscr{N}_j$ ($j = 1,2$). Notice that $N_1 = M_1 + \cdots + M_K$ is the total number of nodes lying on all the interfaces Γ_i, whereas N_2 is the number of the remaining nodes minus one (P_0). Consequently, for a fine mesh, N_1 should be significantly smaller than N_2.

Let

$$u_1 := \big(u(P_i)\big)_{P_i\in\mathscr{N}_1} \in \mathbb{R}^{N_1} \qquad \text{and} \qquad u_2 := \big(u(P_i)\big)_{P_i\in\mathscr{N}_2} \in \mathbb{R}^{N_2}.$$

The matrix form of the discrete problem given by Eq. 7 reads as follows:

$$\begin{pmatrix} A_{11} & A_{12} \\ A_{21} & A_{22} \end{pmatrix} \begin{pmatrix} u_1 \\ u_2 \end{pmatrix} = \begin{pmatrix} \Lambda B_{11} & 0 \\ 0 & 0 \end{pmatrix} \begin{pmatrix} u_1 \\ u_2 \end{pmatrix}, \tag{9}$$

where

$$A_{rs} := \left(\int_\Omega \nabla\beta_i \cdot \nabla\beta_j \right)_{P_i\in\mathscr{N}_r, P_j\in\mathscr{N}_s}, \quad r,s = 1,2,$$

with $\{\beta_i\}_{P_i\in\mathscr{N}}$ being the nodal basis (i.e., $\beta_i(P_j) = \delta_{ij}$), Λ is a diagonal matrix given by

$$\Lambda := \begin{pmatrix} \lambda_1 I_{M_1\times M_1} & & \\ & \ddots & \\ & & \lambda_K I_{M_K\times M_K} \end{pmatrix}, \qquad \text{with } \lambda_i := \frac{\rho\omega_h^2}{k_i - m_i\omega_h^2}, \quad i = 1,\dots,K, \tag{10}$$

($I_{M_i\times M_i}$ denotes the $M_i \times M_i$ identity matrix), and

$$B_{11} := \begin{pmatrix} B^{(1)} & & \\ & \ddots & \\ & & B^{(K)} \end{pmatrix},$$

with $B^{(l)} \in \mathbb{R}^{M_l\times M_l}$ defined by

$$B^{(l)} := \left(\left(\int_{\Gamma_l} \beta_i n \right) \cdot \left(\int_{\Gamma_l} \beta_j n \right) \right)_{P_i,P_j\in\mathscr{N}^{(l)}}, \qquad l = 1,\cdots,K.$$

Our goal is to transform Eq. 9 into a standard symmetric generalized eigenvalue problem of size $2K$ (which is known to be the number of solutions of this problem).

We observe that the matrix on the left hand side of Eq. 9 is symmetric and positive definite. Then, since the submatrix A_{22} is invertible (indeed, symmetric and positive definite, too), by eliminating u_2 from Eq. 9 we arrive at

$$Cu_1 = \Lambda B_{11} u_1, \tag{11}$$

with $C := A_{11} - A_{12}A_{22}^{-1}A_{21}$.

This problem is equivalent to Eq. 9. Notice that although the matrix C is not sparse, its dimension is N_1 and, hence, as stated above, significantly smaller than the size N_1+N_2 of Eq. 9. Moreover, in actual computations, the matrix A_{22}^{-1} is not explicitly computed. In fact, the columns of $A_{22}^{-1}A_{21}$ are obtained by solving N_1 linear systems with the same matrix $A_{22} \in \mathbb{R}^{N_2 \times N_2}$, which is sparse, symmetric and positive definite.

As a second step, we compute a complete diagonalization of the matrix B_{11}. As far as the mesh has no triangles with vertices lying on two different Γ_i, this matrix is block diagonal with K full diagonal blocks, the dimension of each one being M_i. Thus, any standard eigensolver for symmetric matrices (QR, for instance) can be conveniently used for each diagonal block $B^{(i)}$ and provide us with orthogonal matrices $Q^{(i)}$ such that

$$Q^{(i)\mathrm{t}} B^{(i)} Q^{(i)} = D^{(i)} := \operatorname{diag}\left\{\mu_1^{(i)}, \mu_2^{(i)}, 0, \ldots, 0\right\},$$

with $\mu_1^{(i)} \neq 0$ and $\mu_2^{(i)} \neq 0$, $1 \leq i \leq K$.

Thus, if we define

$$Q := \begin{pmatrix} Q^{(1)} & & \\ & \ddots & \\ & & Q^{(K)} \end{pmatrix},$$

we have that

$$Q^{\mathrm{t}} B_{11} Q = D,$$

with

$$D = \begin{pmatrix} D^{(1)} & & \\ & \ddots & \\ & & D^{(K)} \end{pmatrix}.$$

Let $v := Q^{\mathrm{t}} u_1$ and $S := Q^{\mathrm{t}} C Q$. Since $Q^{\mathrm{t}} \Lambda Q = \Lambda$ (because $Q^{(i)\mathrm{t}}(\lambda_i I) Q^{(i)} = \lambda_i I$), Eq. 11 is equivalent to the following one:

$$Sv = \Lambda D v. \tag{12}$$

Matrix D is diagonal with only $2K$ non-zero diagonal entries:

$\mu_1^{(1)}, \mu_2^{(1)}, \ldots, \mu_1^{(K)}, \mu_2^{(K)}$.

Let P be a permutation matrix such that

$$\tilde{D} := P^{\mathrm{t}} D P = \begin{pmatrix} \tilde{D}_{11} & 0 \\ 0 & 0 \end{pmatrix}, \qquad \text{with} \qquad \tilde{D}_{11} := \operatorname{diag}\left\{ \mu_1^{(1)}, \mu_2^{(1)}, \ldots, \mu_1^{(K)}, \mu_2^{(K)} \right\}.$$

Then, Eq. 12 is equivalent to

$$\tilde{S}\tilde{v} = \tilde{\Lambda}\tilde{D}\tilde{v}, \tag{13}$$

where $\tilde{S} := P^{\mathrm{t}} S P$, $\tilde{v} := P^{\mathrm{t}} v$, $\tilde{\Lambda} := P^{\mathrm{t}} \Lambda P$ and $\tilde{D}$ is as defined above.
Since Λ is diagonal, $\tilde{\Lambda}$ is diagonal too and it can be decomposed in blocks as follows:

$$\tilde{\Lambda} = \begin{pmatrix} \tilde{\Lambda}_{11} & 0 \\ 0 & \tilde{\Lambda}_{22} \end{pmatrix}, \qquad \text{with} \qquad \tilde{\Lambda}_{11} := \operatorname{diag}\{\lambda_1, \lambda_1, \ldots, \lambda_K, \lambda_K\}.$$

This leads to the following block decomposition of Eq. 13:

$$\begin{pmatrix} \tilde{S}_{11} & \tilde{S}_{12} \\ \tilde{S}_{21} & \tilde{S}_{22} \end{pmatrix} \begin{pmatrix} \tilde{v}_1 \\ \tilde{v}_2 \end{pmatrix} = \begin{pmatrix} \tilde{\Lambda}_{11} & 0 \\ 0 & \tilde{\Lambda}_{22} \end{pmatrix} \begin{pmatrix} \tilde{D}_{11} & 0 \\ 0 & 0 \end{pmatrix} \begin{pmatrix} \tilde{v}_1 \\ \tilde{v}_2 \end{pmatrix} = \begin{pmatrix} \tilde{\Lambda}_{11}\tilde{D}_{11} & 0 \\ 0 & 0 \end{pmatrix} \begin{pmatrix} \tilde{v}_1 \\ \tilde{v}_2 \end{pmatrix}.$$

Now, by eliminating $\tilde{v}_2$ we arrive at

$$\left(\tilde{S}_{11} - \tilde{S}_{12}\tilde{S}_{22}^{-1}\tilde{S}_{21} \right) \tilde{v}_1 = \tilde{\Lambda}_{11}\tilde{D}_{11}\tilde{v}_1. \tag{14}$$

Let $T := \tilde{S}_{11} - \tilde{S}_{12}\tilde{S}_{22}^{-1}\tilde{S}_{21}$ (notice that T is a symmetric matrix). Since $\tilde{\Lambda}_{11}^{-1} = \frac{1}{\rho\omega_h^2}K - \frac{1}{\rho}M$, with

$K := \operatorname{diag}\{k_1, k_1, \ldots, k_K, k_K\}$ and $M := \operatorname{diag}\{m_1, m_1, \ldots, m_K, m_K\}$,

an easy calculation shows that Eq. 14 is equivalent to the following one:

$$KT\tilde{v}_1 = \omega_h^2 \left(\rho\tilde{D}_{11} + MT \right) \tilde{v}_1. \tag{15}$$

Finally, defining $w := T\tilde{v}_1$, we can rewrite Eq. 15 as follows:

$$\tilde{D}_{11}^{-1} K w = \omega_h^2 \left(\rho T^{-1} + \tilde{D}_{11}^{-1} M \right) w,$$

which is a generalized eigenvalue problem of size $2K$, with both matrices symmetric and positive definite (moreover, the matrix in the left hand side is diagonal). Thus, this is a well posed (and very small) problem that can be efficiently solved by any standard eigensolver.

4 Numerical experiments

In this section we present some numerical results which allow us to assess the performance of the proposed *hp* adaptive refinement strategy.

First of all, let us remark that the optimal meshes for computing different eigenpairs do not necessarily coincide. In fact, the refinement level of these optimal meshes on different parts of the domain depend on the localization and strength of the singularities of the corresponding eigenfunctions, which is not the same for all of them. Thus, the adaptive scheme has to be used separately for each eigenpair.

The color palette, used in the figures, indicates the polynomial degree of each element.

4.1 Test 1: L-shaped cavity with different shape tubes

In this first test we have considered two octagonal tubes and a quadrilateral one within an L-shaped cavity. The domain, the position of the tubes and the initial mesh, with quadratic finite elements in all triangles, is shown in Fig. 2. The fluid density ρ is set to one, whereas the physical parameters m_i and k_i are the same for all tubes and also equal to one. Note that, with these parameters, $\lambda_i = \lambda$ for $i = 1,2,3$ (cf. Eq. 10). The second vibration mode is selected to perform the adaptive process.

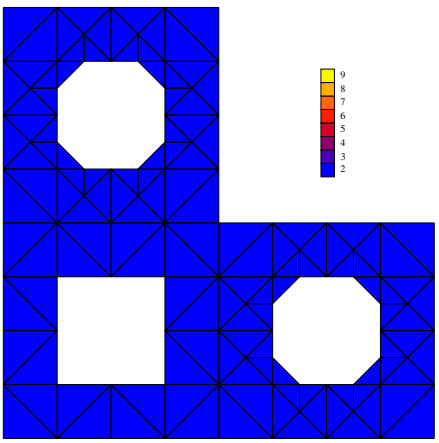

Figure 2: Test 1. Domain and initial mesh for the L-shaped cavity with different shape tubes.

In this numerical example the control parameters appearing in the algorithm, have been chosen as follows: $\theta = 0.5$, $\gamma_h = 20$, $\gamma_p = 0.4$ and $\gamma_n = 2.5$. In this case, the

fluid domain has reentrant angles at the vertices of the tubes, and at the reentrant vertex of the external boundary, producing singularities which compete against each other in the refinement process.

Fig. 3 shows the meshes obtained with the adaptive *hp* algorithm corresponding to step 12 and 24 of the refinement procedure.

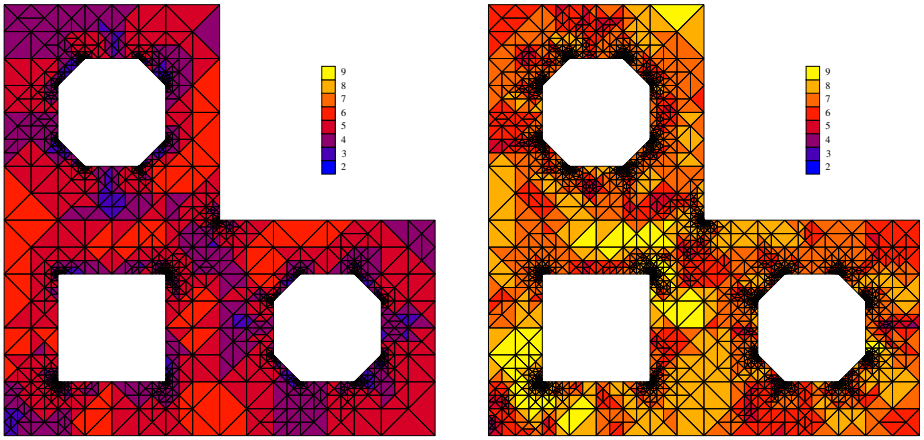

Figure 3: Test 1. Refined meshes: step 12 (left) and 24 (right)

The behavior of the adaptive algorithm in the neighborhood of the different singularities appearing in this example can be appreciated from Fig. 4 to Fig. 6. These figures show sequences of zooms of the mesh at step 24 around different singular points: one of the reentrant angles of the bottom octagon in Fig. 4, the top right corner of the square in Fig. 5 and the reentrant vertex of the rigid cavity in Fig. 6. The last zoom enlarges the original one 10^4 times in Fig. 4, 10^6 times in Fig. 5 and 10^5 times in Fig. 6. Therefore, we observe from these figures that the smallest elements near the vertex in Fig. 6 are approximately ten times larger than those in Fig. 5, but ten times smaller than those in Fig. 4. This indicates that, in this case, the dominant singularity appears at the vertex of the square. Moreover, in all cases we observe the typical *hp* adaptive behavior: the closer to the singularity the more dominant the *h*-refinement is and in the elements nearest the singularity there is no *p*-refinement at all.

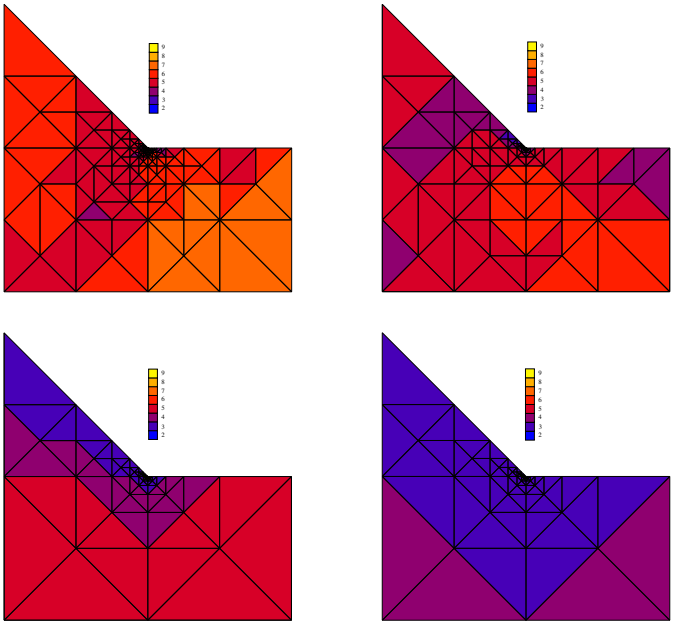

Figure 4: Test 1. Angle at a corner of an octagonal tube. Refined mesh: step 24. Successive zooms

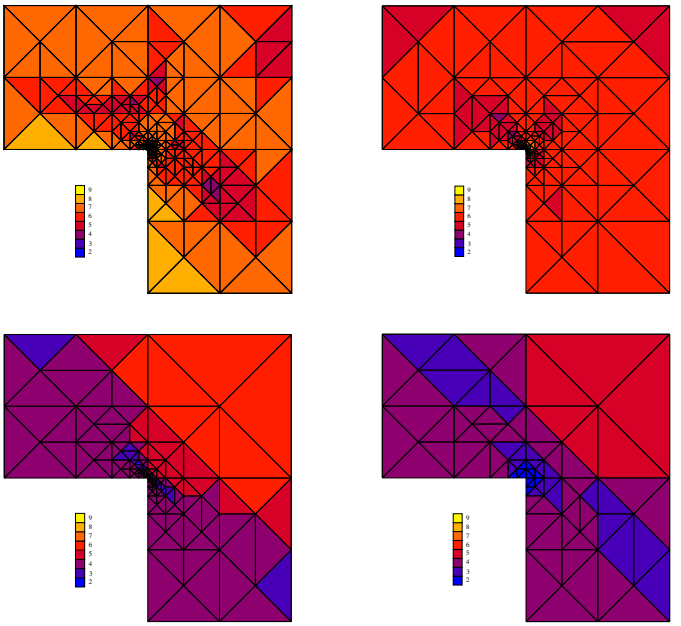

Figure 5: Test 1. Angle at a corner of the square tube. Refined mesh: step 24. Successive zooms

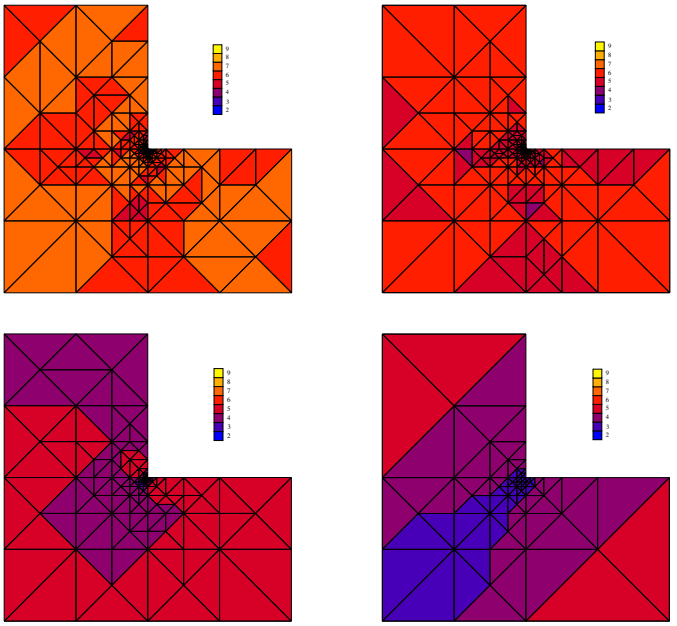

Figure 6: Test 1. Reentrant angle of the L-shaped cavity. Refined mesh: step 24. Successive zooms

Fig. 7 shows the velocity potential obtained at the last step and the fluid velocity field computed from this potential. The arrows at the center of each tube show the tubes velocities.

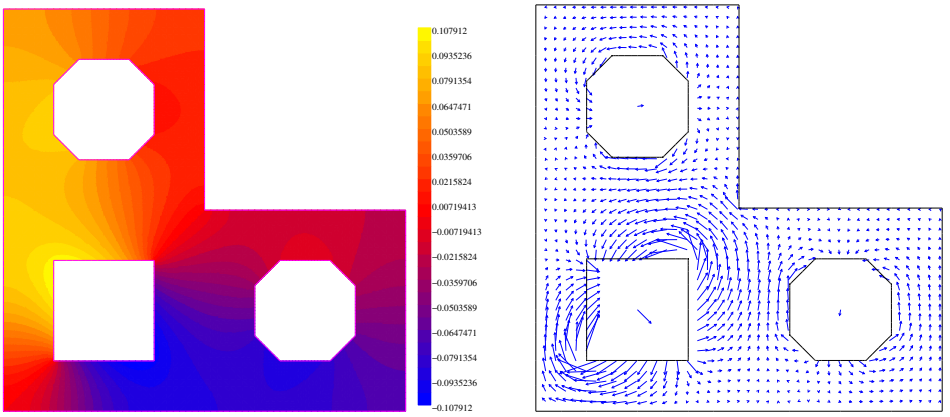

Figure 7: Test 1. Velocity potential (left) and fluid velocity field (right)

It is known that a proper combination of h and p refinement allows to obtain an exponential rate of convergence in terms of a fractional power of the number N of degrees of freedom in the finite element approximation. Fig. 8 shows a plot of $\log(\eta_\Omega)$ versus $\sqrt[3]{N}$, which shows that the estimated error behaves asymptotically in this test as follows:

$$\eta_\Omega \approx \kappa_1 e^{-\alpha \sqrt[3]{N}}.$$

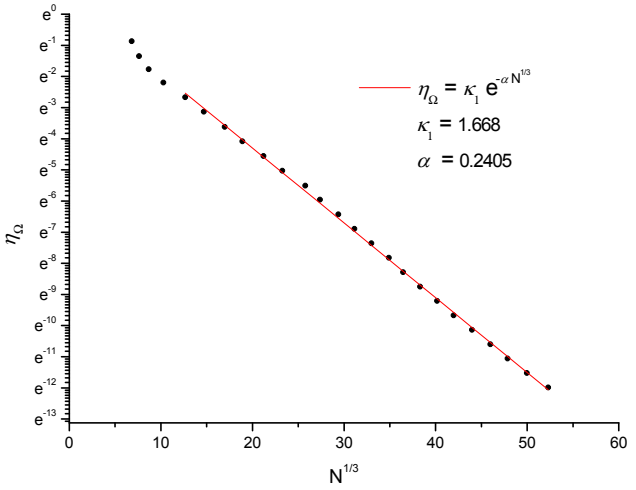

Figure 8: Test 1. η_Ω (logarithmic scale) versus $\sqrt[3]{N}$

No analytical solution is available in this case to check if the actual error also attains an exponential rate of convergence. To provide some numerical evidence of such a behavior, we have estimated the error of the computed eigenvalues by using as 'exact' a more accurate approximation obtained by an extrapolation procedure. To do this, we have used the fact that the computed eigenvalues are expected to converge with a double order and we have determined the parameters λ, κ_2 and α in the model

$$\lambda_h = \lambda + \kappa_2 \mathrm{e}^{-2\alpha \sqrt[3]{N}},$$

by means of a weighted least-squares fitting. The weights have been chosen so that the more accurate the computed values λ_h (i.e., the larger the number of degrees

of freedom of the used mesh), the more significant the role in the fitting. Since we found that the residuals of these meshes are approximately proportional to $e^{-2\alpha\sqrt[3]{N}}$, we chose the weights equal to $e^{4\alpha\sqrt[3]{N}}$. Thus, we have obtained a fitted value $\lambda = 0.136286733762653$, which we have used to plot $\log(\lambda_h - \lambda)$ versus $\sqrt[3]{N}$. This plot is shown in Fig. 9, where a linear dependence can be clearly seen for sufficiently large values of N.

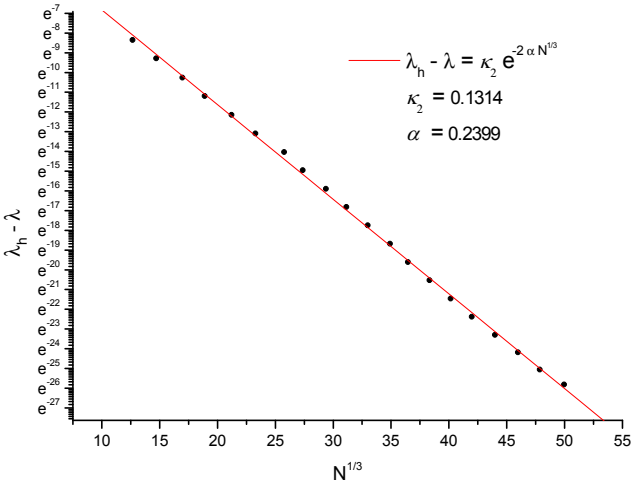

Figure 9: Test 1. $\lambda_h - \lambda$ (logarithmic scale) versus $\sqrt[3]{N}$

Note that the computed values of α in both fittings are quite close: $\alpha = 0.2405$ in the former (cf. Fig. 8) and $\alpha = 0.2399$ in the latter (cf. Fig. 9). This excellent agreement provides a sound numerical evidence of the fact that the error estimate behaves asymptotically as the actual error.

On the other hand, the convergence behavior shown in Fig. 9 is coherent with the theoretically expected exponential decay of the error with respect to the number of degrees of freedom. In fact, the obtained convergence rate $\exp(-\alpha\sqrt[3]{N})$ is typical for the *hp* version of the finite element method for source elliptic problems with piecewise analytic data in the presence of corner singularities [Babuška and Guo (1988)]. Let us remark that this convergence rate does not agree with what was reported in our previous paper [Armentano, Padra, Rodríguez, and Scheble (2011)], where an apparently improved rate $\exp(-\alpha\sqrt{N})$was observed for a similar experiment with identical tubes.

4.2 Test 2: Bundle of circular tubes with different physical parameters within a quadrilateral cavity

As a second test, we have computed all the vibration modes of a system closer to the actual applications: four circular tubes with different physical parameters immersed in a fluid occupying a quadrilateral cavity. The position of the tubes and the initial mesh, with quadratic finite element in all triangles, is shown in Fig. 10.

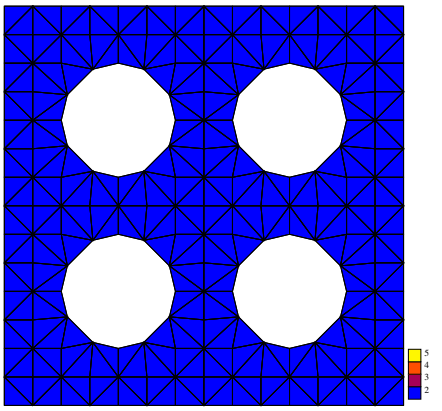

Figure 10: Test 2. Domain and initial mesh of the square cavity with four tubes.

In this case, the fluid density has been taken $\rho = 1$ and the physical parameters of the tubes as follows: mass $m_i = 1$, $i = 1,\ldots,4$ and stiffness $k_1 = k_4 = 1.05$ and $k_2 = k_3 = 1$. The control parameters appearing in the algorithm, have been chosen as follows: $\theta = 0.75$, $\gamma_h = 8$, $\gamma_p = 0.2$ and $\gamma_n = 1$.

We report in Tab. 2 the eight frequencies obtained after 8 steps of refinement.

Table 2: Test 2. Angular vibration frequencies

Mode	ω
1	0.9619
2	0.9627
3	0.9653
4	0.9661
5	0.9895
6	0.9921
7	0.9930
8	1.0026

The sequence of meshes obtained during the adaptive process not only depends on the geometry, but also on the physical parameters of the tubes. This is clear from the fact that different rigidities and masses can significantly change the motion of tubes, and therefore, the type of singularities present at their boundaries.

Fig. 11 shows the meshes obtained after 8 steps of the *hp*-adaptive scheme for a couple of vibration modes. Let us recall that each vibration mode has to be computed separately. It can be seen from this figure that the corresponding optimal *hp* meshes actually do not coincide.

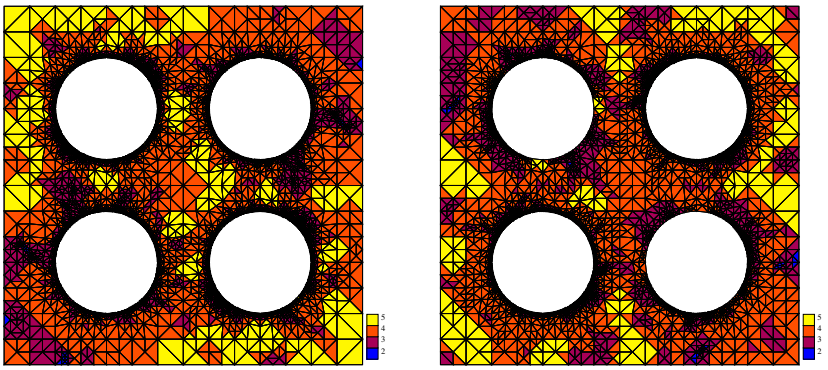

Figure 11: Test 2. Refined meshes at step 8: first mode (left) and sixth mode (right)

Fig. 12 shows the velocity potential computed with the final mesh of the adaptive process for the same vibrations modes. Fig. 13 shows the corresponding fluid velocity fields. The arrows at the center of each tube show the velocities of the tubes motion.

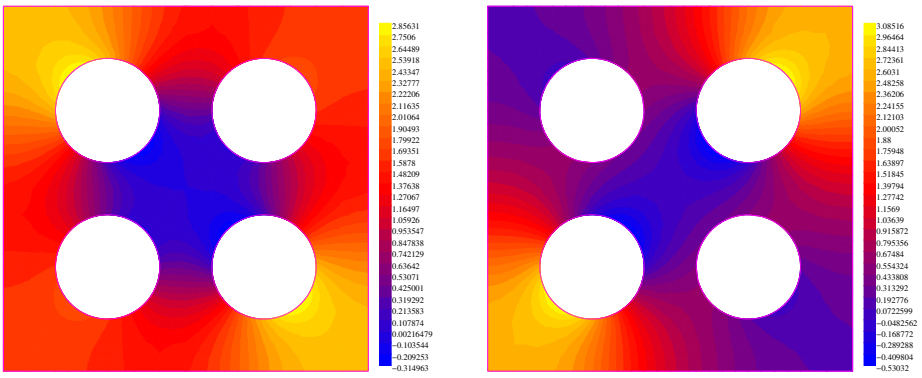

Figure 12: Test 2. Velocity potential for the first mode (left) and the sixth mode (right)

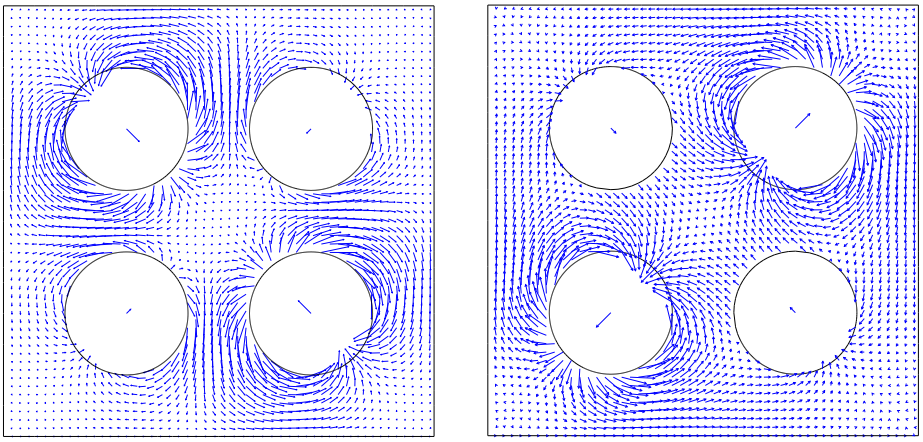

Figure 13: Test 2. Fluid velocity field for the first mode (left) and the sixth mode (right)

5 Conclusions

An *hp* finite element method has been proposed to compute the free vibration modes of a bundle of different tubes immersed in an incompressible fluid contained in a rigid cavity. This leads to a non-standard eigenvalue problem, when the tubes are not all identical.

We have introduced an algebraic procedure to transform the resulting eigenvalue problem into a small-size standard one, which can be solved with classical eigensolvers.

We have proposed an a posteriori error indicator and an adaptive algorithm based on this indicator, which allows refining some of the elements and increasing the polynomial degree in others at each step.

The reported numerical experiments for different cavities and different shape, mass and stiffness of tubes show the good performance of the error indicator and of the adaptive scheme. The sequence of meshes obtained during the adaptive process not only depends on the geometry, but also on the physical parameters of the tubes. Numerical evidence of the theoretically expected exponential convergence is also reported.

Acknowledgement: This work was partially supported by ANPCyT (Argentina) under grant PICT 2006-01307. The first author was partially supported by ANPCyT (Argentina) under grant PICT-2007-00910 and by Universidad de Buenos Aires (Argentina) under grant X007. The first and second authors are members

of CONICET (Argentina). The third author was partially supported by BASAL projects, CMM, Universidad de Chile (Chile).

References

Armentano, M. G.; Padra, C. (2008): A posteriori error estimates for the Steklov eigenvalue problem. *Appl. Numer. Math.*, vol. 58, pp. 593–601.

Armentano, M. G.; Padra, C.; Rodríguez, R.; Scheble, M. (2011): An *hp* finite element adaptive scheme to solve the Laplace model for fluid-solid vibrations. *Comput Methods Appl. Mech. Engrg*, vol. 200, pp. 178–188.

Azaiez, M.; Deville, M. O.; Gruber, R.; Mund, E. H. (2008): A new *hp* method for the $-\mathrm{grad}(\mathrm{div})$ operator in non-Cartesian geometries. *Appl. Numer. Math.*, vol. 58, pp. 985–998.

Babuška, I.; Guo, B. Q. (1988): The *h-p* version of the finite element method for domains with curved boundaries. *SIAM J. Numer. Anal.*, vol. 25, pp. 837–861.

Bermúdez, A.; Durán, R.; Rodríguez, R. (1997): Finite element solution of incompressible fluid-structure vibration problems. *Internat. J. Numer. Methods Engrg.*, vol. 40, pp. 1435–1448.

Bermúdez, A.; Rodríguez, R.; Santamarina, D. (2000): A finite element solution of an added mass formulation for coupled fluid-solid vibrations. *Numer. Math.*, vol. 87, pp. 201–227.

Boffi, D. (2007): Approximation of eigenvalues in mixed form, discrete compactness property, and application to *hp* mixed finite elements. *Comput. Methods Appl. Mech. Engrg.*, vol. 196, pp. 3672–3681.

Boffi, D.; Costabel, M.; Dauge, M.; Demkowicz, L. (2006): Discrete compactness for the *hp* version of rectangular edge finite elements. *SIAM J. Numer. Anal.*, vol. 44, pp. 979–1004.

Conca, C.; Osses, A.; Planchard, J. (1998): Asymptotic analysis relating spectral models in fluid-solid vibrations. *SIAM J. Numer. Anal.*, vol. 35, pp. 1020–1048.

Conca, C.; Planchard, J.; Vanninathan, M. (1995): *Fluid and Periodic Structures*. Masson, Paris.

Durán, R. G.; Gastaldi, L.; Padra, C. (1999): A posteriori error estimators for mixed approximations of eigenvalue problems. *Math. Models Methods Appl. Sci.*, vol. 9, pp. 1165–1178.

Durán, R. G.; Padra, C.; Rodríguez, R. (2003): A posteriori error estimates for the finite element approximation of eigenvalue problems. *Math. Models Methods Appl. Sci.*, vol. 13, pp. 1219–1229.

IAEA (2005): Design of the reactor core for nuclear power plants. *IAEA Safety Standards Series No. NS-G-1.12*.

Larson, M. G. (2000): A posteriori and a priori error analysis for finite element approximations of self-adjoint elliptic eigenvalue problems. *SIAM J. Numer. Anal.*, vol. 38, pp. 608–625.

Lovadina, C.; Lyly, M.; Stenberg, R. (2009): A posteriori estimates for the Stokes eigenvalue problem. *Numer. Methods PDEs*, vol. 25, pp. 244–257.

Melenk, J. M.; Wohlmuth, B. I. (2001): On residual-based a posteriori error estimation in *hp*-FEM. *Adv. Comput. Math.*, vol. 15, pp. 311–331.

Morand, H. J. P.; Ohayon, R. (1995): *Fluid-Structure Interaction*. John Wiley & Sons, Chichester.

Planchard, J. (1983): Eigenfrequencies of a tube bundle placed in a confined fluid. *Comput. Methods Appl. Mech. Engrg.*, vol. 30, pp. 75–93.

Planchard, J.; Ibnou-Zahir, M. (1983): Natural frequencies of tube bundle in an uncompressible fluid. *Comput. Methods Appl. Mech. Engrg.*, vol. 41, pp. 47–68.

Verfürth, R. (1996): *A Review of A Posteriori Error Estimation and Adaptive Mesh-Refinement Techniques*. Wiley & Teubner.